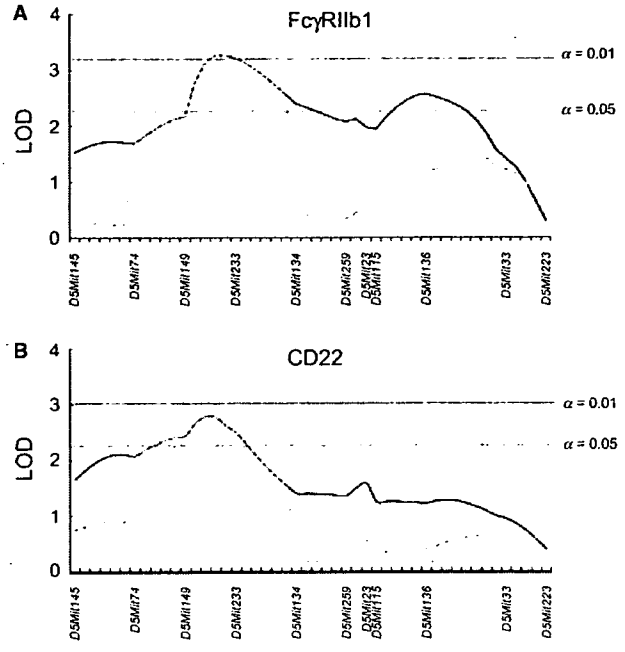

Figure 4 Plots of the logarithmic odds (LOD) scores of QTL on chromosome 5 for the expression of FcγRIIb1 (A) and CD22 (B) transcript in the spleen of MCF_2 mice. Solid and broken lines indicate the results from interval mapping and composite interval mapping analysis respectively. We adopted the composite interval mapping method of Model 6 in the Windows QTL Cartographer (V2.5) software. The control marker number and window size were 5 and 10 cM respectively. Horizontal lines indicate the threshold levels of significant LOD determined by the permutation test installed in this programme (1000 times permutations, α = 0.01 for upper line, α = 0.05 for lower line). Genetic positions of MIT markers are indicated on the horizontal axis.

Acknowledgment

The authors thank Mrs H. Ohura for technical assistances, the members of the Integrated Center for Sciences (INCS), Ehime University for animal breeding, and Mrs N. Fujisawa for secretarial assistance. This study was supported by Grants-in-Aid for Scientific Research from the Ministry of Education, Science, Sports, and Culture of Japan to MO (19390108 and 19659096).

References

1 Andrews BS, Eisenberg RA, Theofilopoulos AN *et al.* Spontaneous murine lupus-like syndromes. Clinical and immunopathological manifestations in several strains. *J Exp Med* 1978;148:1198–215.

2 Morse HC III, Davidson WF, Yetter RA, Murphy ED, Roths JB, Coffman RL. Abnormalities induced by the mutant gene lpr: expansion of a unique lymphocyte subset. *J Immunol* 1982;129:2612–5.

3 Jonsson R, Tarkowski A, Backman K, Holmdahl R, Klareskog L. Sialadenitis in the MRL-l mouse: morphological and immunohistochemical characterization of resident and infiltrating cells. *Immunology* 1987;60:611–6.

4 Hang L, Theofilopoulos AN, Dixon FJ. A spontaneous rheumatoid arthritis-like disease in MRL/l mice. *J Exp Med* 1982;155:1690–701.

5 Watanabe-Fukunaga R, Brannan CI, Copeland NG, Jenkins NA, Nagata S. Lymphoproliferation disorder in mice explained by defects in Fas antigen that mediates apoptosis. *Nature* 1992;356:314–7.

6 Izui S, Kelley VE, Masuda K, Yoshida H, Roths JB, Murphy ED. Induction of various autoantibodies by mutant gene lpr in several strains of mice. *J Immunol* 1984;133:227–33.

7 Kelley VE, Roths JB. Interaction of mutant lpr gene with background strain influences renal disease. *Clin Immunol Immunopathol* 1985;37:220–9.

8 Nose M, Nishihara M, Fujii H. Genetic basis of the complex pathological manifestations of collagen disease: lessons from MRL/lpr and related mouse models. *Int Rev Immunol* 2000;19:473–98.

9 Zhang MC, Misu N, Furukawa H *et al.* An epistatic effect of the female specific loci on the development of autoimmune vasculitis and antinuclear autoantibody in murine lupus. *Ann Rheum Dis* 2006;65:495–500.

10 Roark JH, Kuntz CL, Nguyen KA, Mandik L, Cattermole M, Erikson J. B cell selection and allelic exclusion of an anti-DNA Ig transgene in MRL-lpr/lpr mice. *J Immunol* 1995;154:4444–55.

11 Kench JA, Russell DM, Nemazee D. Efficient peripheral clonal elimination of B lymphocytes in MRL/lpr mice bearing autoantibody transgenes. *J Exp Med* 1998;188:909–17.

12 Mandik-Nayak L, Seo S, Eaton-Bassiri A, Allman D, Hardy RR, Erikson J. Functional consequences of the developmental arrest and follicular exclusion of anti-double-stranded DNA B cells. *J Immunol* 2000;164:1161–8.

13 Jyonouchi H, Kincade PW, Good RA. Age-dependent changes in B lymphocyte lineage cell populations of autoimmune-prone BXSB mice. *J Immunol* 1985;134:858–64.

14 Nijnik A, Ferry H, Lewis G *et al.* Spontaneous B cell hyperactivity in autoimmune-prone MRL mice. *Int Immunol* 2006;18:1127–37.

15 Bolland S, Ravetch JV. Spontaneous autoimmune disease in Fc(gamma)RIIB-deficient mice results from strain-specific epistasis. *Immunity* 2000;13:277–85.

16 Cornall RJ, Cyster JG, Hibbs ML *et al.* Polygenic autoimmune traits: Lyn, CD22, and SHP-1 are limiting elements of a biochemical pathway regulating BCR signaling and selection. *Immunity* 1998;8:497–508.

17 Jiang Y, Hirose S, Abe M *et al.* Polymorphisms in IgG Fc receptor IIB regulatory regions associated with autoimmune susceptibility. *Immunogenetics* 2000;51:429–35.

18 Mary C, Laporte C, Parzy D *et al.* Dysregulated expression of the Cd22 gene as a result of a short interspersed nucleotide element insertion in Cd22a lupus-prone mice. *J Immunol* 2000;165:2987–96.

19 Kyogoku C, Dijstelbloem HM, Tsuchiya N *et al.* Fcgamma receptor gene polymorphisms in Japanese patients with systemic lupus erythematosus: contribution of FCGR2B to genetic susceptibility. *Arthritis Rheum* 2002;46:1242–54.

20 Miyazaki T, Ono M, Qu WM *et al.* Implication of allelic polymorphism of osteopontin in the development of lupus nephritis in MRL/lpr mice. *Eur J Immunol* 2005;35:1510–20.

21 Kamogawa J, Terada M, Mizuki S *et al.* Arthritis in MRL/lpr mice is under the control of multiple gene loci with an allelic combination derived from the original inbred strains. *Arthritis Rheum* 2002;46:1067–74.

22 Mori S, Zhang MC, Tanda N *et al.* Genetic characterisation of spontaneous ankylosing arthropathy with unique inheritance from Fas-deficient strains of mice. *Ann Rheum Dis* 2006;65:1273–8.

23 Zhang MC, Mori S, Date F, Furukawa H, Ono M. A non-major histocompatibility locus determines tissue specificity in the pathogenic process underlying synovial proliferation in a mouse arthropathy model. *Ann Rheum Dis* 2007;66:242–5.

24 Qu WM, Miyazaki T, Terada M *et al.* Genetic dissection of vasculitis in MRL/lpr lupus mice: a novel susceptibility locus involving the CD72c allele. *Eur J Immunol* 2000;30:2027–37.

25 Yamada A, Miyazaki T, Lu LM *et al.* Genetic basis of tissue specificity of vasculitis in MRL/lpr mice. *Arthritis Rheum* 2003;48:1445–51.
26 Nishihara M, Terada M, Kamogawa J *et al.* Genetic basis of autoimmune sialadenitis in MRL/lpr lupus-prone mice: additive and hierarchical properties of polygenic inheritance. *Arthritis Rheum* 1999;42:2616–23.
27 Lander E, Kruglyak L. Genetic dissection of complex traits: guidelines for interpreting and reporting linkage results. *Nat Genet* 1995;11:241–7.
28 Zeng ZB. Precision mapping of quantitative trait loci. *Genetics* 1994;136:1457–68.
29 Churchill GA, Doerge RW. Empirical threshold values for quantitative trait mapping. *Genetics* 1994;138:963–71.
30 Ravetch JV, Luster AD, Weinshank R *et al.* Structural heterogeneity and functional domains of murine immunoglobulin G Fc receptors. *Science* 1986;234:718–25.
31 Amigorena S, Bonnerot C, Choquet D, Fridman WH, Teillaud JL. Fc gamma RII expression in resting and activated B lymphocytes. *Eur J Immunol* 1989;19:1379–85.
32 Stephan RP, Sanders VM, Witte PL. Stage-specific alterations in murine B lymphopoiesis with age. *Int Immunol* 1996;8:509–18.
33 Stephan RP, Lill-Elghanian DA, Witte PL. Development of B cells in aged mice: decline in the ability of pro-B cells to respond to IL-7 but not to other growth factors. *J Immunol* 1997; 158:1598–609.
34 Stephan RP, Reilly CR, Witte PL. Impaired ability of bone marrow stromal cells to support B-lymphopoiesis with age. *Blood* 1998;91:75–88.
35 Kaisho T, Ishikawa J, Oritani K *et al.* BST-1, a surface molecule of bone marrow stromal cell lines that facilitates pre-B-cell growth. *Proc Natl Acad Sci USA* 1994;91:5325–9.
36 Kumagai M, Coustan-Smith E, Murray DJ *et al.* Ligation of CD38 suppresses human B lymphopoiesis. *J Exp Med* 1995;181:1101–10.
37 Kitanaka A, Ito C, Nishigaki H, Campana D. CD38-mediated growth suppression of B-cell progenitors requires activation of phosphatidylinositol 3-kinase and involves its association with the protein product of the c-cbl proto-oncogene. *Blood* 1996;88: 590–8.
38 Yamashita Y, Miyake K, Kikuchi Y *et al.* A monoclonal antibody against a murine CD38 homologue delivers a signal to B cells for prolongation of survival and protection against apoptosis *in vitro*: unresponsiveness of X-linked immunodeficient B cells. *Immunology* 1995;85:248–55.
39 Funaro A, Morra M, Calosso L, Zini MG, Ausiello CM, Malavasi F. Role of the human CD38 molecule in B cell activation and proliferation. *Tissue Antigens* 1997;49:7–15.

ELSEVIER

Ultrasound in Med. & Biol., Vol. 34, No. 3, pp. 425–434, 2008

0301-5629/08/$–see front matter

doi:10.1016/j.ultrasmedbio.2007.09.004

● *Original Contribution*

HERPES SIMPLEX VIRUS THYMIDINE KINASE-MEDIATED SUICIDE GENE THERAPY USING NANO/MICROBUBBLES AND ULTRASOUND

ATSUKO AOI,*† YUKIKO WATANABE,* SHIRO MORI,‡ MASAHIKO TAKAHASHI,† GEORGES VASSAUX,§‖ and TETSUYA KODAMA*

*Biomedical Engineering Research Organization, Tohoku University, †Graduate School of Dentistry, Tohoku University, ‡Tohoku University Hospital, Sendai, Japan; and §INSERM CIC-004, ‖Institut des maladies de l'Appareil Digestif, CHU Hotel Dieu, Nantes, France

(*Received* 12 *January* 2007, *revised* 25 *June* 2007, *in final form* 5 *September* 2007)

Abstract—A physical method using ultrasound (US) and nano/microbubbles (NBs) can deliver exogenous molecules noninvasively into a specific target site. In this study, we evaluated the application of this technology to cancer gene therapy using prodrug activation therapy. Low-intensity pulsed ultrasound (1 MHz; 1.3 W/cm^2) and NBs were used to transduce the herpes simplex thymidine kinase (HSV*tk*) gene *in vitro*, leading to gene transfer. The addition of ganciclovir (GCV) to the transduced cells led to HSV*tk*/GCV-dependent cell death mediated by apoptosis. This technology was then assessed *in vivo*, using mice bearing subcutaneous tumors (1 MHz; 3.0 W/cm^2). Gene transfer to the tumor, measured by luciferase activity, was transient, with a peak of expression 24 h after transduction, and decreased at 48 h, demonstrating the transient nature of US/NB-mediated gene transfer. The therapeutic potential of this approach was evaluated through repeated intratumoral gene delivery using US/NB-mediated transfer of the HSV*tk* gene, followed by recurrent administration of GCV, using two different experimental treatment protocols. In both cases, dramatic reductions of the tumor size by a factor of four were observed. Altogether, these data demonstrate the potential of US/NB as a new physical gene delivery method for cancer gene therapy. (E-mail: kodama@tubero.tohoku.ac.jp) © **2008 World Federation for Ultrasound in Medicine & Biology.**

Key Words: **Membrane permeability, *In-vivo* imaging, Molecular delivery, Cancer gene therapy.**

INTRODUCTION

Cancer therapy based on gene delivery requires highly efficient molecular delivery methods into a specific target site. One of the physical methods of gene delivery exploits nano/microbubbles (NBs) combined with ultrasound (US). Nano/microbubbles are encapsulated gas bubbles with a radius of <5 μm. The shell membrane consists of albumin, lipid or polymer. The inside gas comprises either air or perfluorocarbons (large molecules have a small diffusion efficiency into liquid, resulting in increased bubble life time) (Chomas et al. 2001; Harvey et al. 2001). These bubbles are not only used as US contrast agent to identify and delineate cardiac anatomy, such as thrombi or clot formation, but they are also used for evaluation of blood pool and blood flow at the microvascular level (Lindner 2004). The mechanical index (MI, defined as the peak negative pressure divided by the square root of the US frequency) of US used in clinical application is 0.05 to 1.9 (McCulloch et al. 2000) and NBs collapse at MI = 0.3 to 0.5 (Ammi et al. 2006; Chen et al. 1995; Wu and Tong 1998). The impulsive pressures generated by either the collapse of NBs or cavitation bubbles created by the collapse of NBs are able to induce a transient permeabilization of cells, followed by the entry of exogenous molecules into cells. This method is not toxic and nonimmunogenic and can be combined with chemotherapy (Pitt et al. 2004).

Suicide gene therapy involves transfer into cancer cells of a gene capable of converting nontoxic prodrugs into cytotoxic drugs. One of the most common approaches uses the herpes simplex virus thymidine kinase (HSV*tk*) gene combined with the prodrug ganciclovir (GCV). The nucleoside analogue GCV is phosphorylated 1,000 times less efficiently by eukaryotic thymidine kinases and experimentally, *in vivo*, GCV is only phosphorylated by cells producing the virus enzyme HSV*tk*

Address correspondence to: Tetsuya Kodama, Ph.D., Professor, Biomedical Engineering Research Organization, Tohoku University, 2–1 Seiryo-machi, Aoba-ku, Sendai 980–8575, Japan. E-mail: kodama@tubero.tohoku.ac.jp

(Keller et al. 1981; Oliver et al. 1985). The product of the reaction (GCV-MP) is then further phosphorylated to GCV-diphosphate (GCV-DP) and GCV-triphosphate (GCV-TP) by endogenous cellular kinases. GCV-TP inhibits competitively the incorporation of dGTP into DNA (Mesnil and Yamasaki 2000), resulting in cell death (Fillat et al. 2003; Mesnil and Yamasaki 2000). Apoptosis has been suggested to be involved in the cell death, which may occur by a pathway independent of p53 (Wallace et al. 1996). In fact, it has been reported that cell lines with mutant p53 expressing HSV*tk* were not resistant to GCV (Vassaux and Martin-Duque 2004; Wallace et al. 1996; Yoon et al. 1999). Cytotoxicity is observed not only in HSV*tk*-positive cells but also in neighboring HSV*tk*-negative cells as a result of the bystander effect. HSV*tk*-negative cells show cytotoxicity *in vitro* when the population of cultured cells contained only 10% HSV*tk*-positive cells (Freeman et al. 1993). This bystander effect is regarded as a transfer phenomenon of the toxic metabolites of GCV from HSV*tk*-positive cells to HSV*tk*-negative cell, in which gap junctional intercellular communication (GJIC) appears crucial.

In the present report, we evaluated the potential of US and NBs as a physical method of gene transfer in cancer gene therapy using the HSV*tk*/GCV system as a therapeutic agent.

MATERIALS AND METHODS

Nano/microbubbles

Two types of NBs, Optison™ (Amersham Health PLC, Oslo, Norway) and lipid-micelle bubbles were used. Both bubbles provided very similar physical chemical properties (size distribution and ζ potential). A report on the systematic comparison of the two reagents is currently in preparation. Optison is an octafluoropropane (C_3F_8)-filled albumin microspheres that has a mean diameter between 3.0 and 4.5 μm (max. 32.0 μm). In this study, the mean concentration was set to the arithmetic average of 6.5×10^8 bubbles/mL. Lipid-micelle bubbles were created in an aqueous dispersion of 2 mg/mL 1,2-distearoyl-sn-glycero-3-phosphocholine (DSPC) (Avanti Polar Lipids, Alabaster, AL, USA) and 1 mg/mL polyethleneglycol-40 stearate (PEG) (Sigma-Aldrich Co., St. Louis, MO, USA) using a 20-kHz sonicator (Vibra Cell, Sonics & Materials, Inc., Danbury, CT, USA) in the presence of C_3F_8 gas (Aoi et al. 2006). The theoretically calculated concentration was 1.6×10^{10} bubbles/mL. The lipid bubble surface that comprised lipid molecules was confirmed by staining lipid molecules with 3 μM FM1–43 (553 nm, Abs: 570 nm, Em., Molecular Probe Inc, Eugene, OR, USA) under an inverted microscope (IX81, Olympus Co., Tokyo, Japan). The bubble size distribution was determined by using a laser diffraction particle size analyzer (particle range of 0.6 nm–7 μm, ELSZ-2, Otsuka Electronics Co. Ltd, Osaka, Japan). The peak diameters expressed in terms of the size distribution of Optison and lipid bubbles were 1689 $\pm$ 150 nm (n = 4) and 1272 $\pm$ 163 nm (n = 7), respectively. Because the volume distribution is proportional to the third power of the size, the peak of the size distribution tends to be measured as a smaller value than that of the volume distribution. The ζ potential of the bubbles was measured by the ELSZ-2 in phosphate-buffered saline without Mg_{2+} and Ca_{2+} (PBS). Zeta potential refers to the electrostatic potential generated by the accumulation of ions at the surface of a bubble that is organized into an electrical double layer. The ζ potential of the Optison and lipid bubble, was –36.9 $\pm$ 2.70 mV (n = 3) and –4.11 $\pm$ 0.74 mV (n = 4), respectively, indicating that Optison have larger mutual impulsive forces and higher stability compared with the lipid bubbles. In our previous experiments, there were no significant differences in *in-vitro* gene activity between Optison and lipid micelle bubbles (data not shown). In the following experiments, lipid-micelle bubbles and Optison were used for *in-vitro* and *in-vivo* experiments, respectively.

Cell preparation

Human lung carcinoma (A549) and murine colon carcinoma (colon26, which was abbreviated as C26 in the text) were obtained from the Cell Resource Center for Biomedical Research, Institute of Development, Aging and Cancer, Tohoku University, Sendai, Japan. Murine breast carcinoma (EMT6) cells were obtained from the American Type Culture Collection (Manassas, VA, USA). Murine breast carcinoma cells (EMT6-luc) stably expressing the firefly luciferase gene were prepared by transfected pEGFPLuc (BD Biosciences, Franklin Lakes, NJ, USA) and Lipofectin Transfer Reagent (Invitrogen, Carlsbad, CA, USA). Human colon carcinoma cells (HT29) were obtained from Cancer Research UK (London, UK), and human colon carcinoma cells (HT29-luc) stably expressing the firefly luciferase gene were obtained from Xenogen (Alameda, CA, USA). A549, C26, HT29 and HT29-luc cells were cultured under standard conditions in RPMI 1640 supplemented with 10% heat-inactivated fetal bovine serum (FBS) (Invitrogen) and 1% L-glutamine-penicillin-streptomycin (Sigma-Aldrich, St. Louis, MO, USA), whereas EMT6 cells and EMT6-luc were cultured in DMEM (Sigma-Aldrich) medium with the same supplements. Cells cultured in a 10-cm culture dish were maintained in a humidified incubator at 37° C under an atmosphere of 5% CO_2 and 95% air.

Plasmids

The luciferase reporter vector pGL3-control (Promega, Madison, WI, USA), which expresses luciferase from SV40 promoter, pGV24 vector in which HSV*tk* expression is driven by the ERBB2 promoter (Vassaux et al. 1999) and pRS303 that does not have any transgene expressed, were used as mock plasmid. pGV24 and pRS303 were referred to as pHSV*tk* and pMock, respectively.

Ultrasound

Two 1-MHz submersible US probes (Fuji Ceramics Co., Fujinomiya, Japan), 12 and 38 mm in diameter, were used for *in-vitro* and *in-vivo* experiments, respectively. Each probe was located in a test chamber (380 × 250 × 130 mm^3) filled with tap water. Each frequency was generated by a multifunction synthesizer (WF1946A; NF Co., Yokohama, Japan), amplified with a high-speed bipolar amplifier (HSA4101; NF Co.). The pressure values were measured by a PVDF needle-hydrophone (PVDF-Z44–1000; Specialty Engineering Associates, Soquel, CA, USA) at a stand-off distance of 1 mm from the transducer surface using a stage control system (Mark-204-MS, Sigma Koki, Tokyo, Japan). The signals from both the amplifier and the hydrophone were recorded into a digital phosphor oscilloscope (Wave Surfer 454, 500 MHz, 1 mol/LΩ (16 pF), LeCroy Co., Chestnut, NY, USA).

In-vitro *transfection by ultrasound and nanobubbles*

In-vitro studies were performed in accordance with the Tohoku University ethical guidelines. A549 (1 × 10^4 cells/well), HT29 (1 × 10^4 cells/well), C26 (2 × 10^4 cells/well) and EMT6 (2 × 10^4 cells/well) cells were seeded in 24-well plates in complete media at 37° C in a 5% CO_2 incubator. The next day, the medium was replaced with fresh media (200 μL), containing pMock (4 μg/mL) or pHSV*tk* (4 μg/mL) with and without NBs (10% v/v). The 24-well plates were located just above the US probe in a test chamber filled with tap water and exposed to the optimized US (intensity: 1.3 W/cm^2, duty ratio: 50%, number of pulse: 2000, exposure time: 10s). The surface of the media was disturbed by US, thus we ignored the effect of standing waves on gene expression. Because cells were seeded into wells alternately, neighboring wells were not exposed to ultrasound at the same time. The plates were incubated for 1 h at 37° C in a 5% CO_2 incubator, supplemented with 800 μL of complete media and then incubated for another 24 h at 37° C in a 5% CO_2 incubator.

In-vitro *sensitivity to GCV assays*

Twenty-four hours after transfection, the media was replaced with complete media (1 mL) containing GCV (0.1–1000 μg/mL, molecular weight 255.2; F. Hoffman-La Roche Ltd., Basel, Switzerland). The plates were incubated for another three to five days at 37° C in a 5% CO_2 incubator. Survival fractions were measured by MTT assay (Kodama et al. 2003; Martinico et al. 2006). Each experiment consisted of six to 15 samples receiving US + NB + GCV with HSV*tk* (or Mock) and six to 15 control samples receiving US and NB. For each experiment, the mean % of treated samples was divided by the mean % of control samples to give a survival fraction. The mean of six to 15 survival fractions was calculated for each condition. The survival fraction of each cell line was measured at the GCV concentration where the highest statistical significant was obtained.

RT-PCR

The total RNAs were reverse-transcribed using the RNA PCR Kit (AMV) (Takara Bio Inc., Tokyo, Japan) according to the manufacturer's instructions (1 μg of total RNA was used). The cDNAs obtained were then subjected to polymerase chain reaction (PCR) amplification (3 min at 94 °C, and 35 cycles of denaturation 95 °C for 60 s, annealing 58.4 °C for 60 s and extension 72 °C for 60 s, followed by 5 min of extension 72 °C) with either HSV*tk*-specific primers (5′-AACAATGGGCATGCCTTATGC-3′; 5′-TTATACAGGTCGCCGTTGGGG-3′, with an expected PCR product of 540 bp) or β-actin–specific primers (5′-CTGTCTGGCGGCACCACCAT-3′; 5′-GCAACTAAGTCATAGTCCGC-3′, with an expected PCR product of 254 bp). The PCR products were then separated on a 2% agarose gel.

Apoptotic assay

Apoptotic cells were detected by fluorescence microscopy (DAPI staining) and TUNEL assay. For DAPI staining, cells incubated in the presence of GCV (10 μg/mL) for 24 h after the treatment of US+NB+ HSV*tk* were stained with DAPI solution (100 ng/mL). For TUNEL assay, cells were harvested at 48 h after treatment, fixed in 4% (w/v) paraformaldehyde with PBS and then washed with PBS and stored in 70% ethanol at –20° C for at least 30 min. The ethanol solution was subsequently removed after centrifugation, and cells were treated with the enzyme terminal deoxynucleotidyl transferase and FITC-labeled dUTP using the Mebstain apoptosis kit from MBL (Nagoya, Japan) according to the manufacturer's protocol. FITC-labeled cells were measured by flow cytometry (FACSCalibur, Becton Dickinson, San Jose, CA, USA). A total of 10,000 events per sample were collected in list mode, and data were analyzed with Cell Quest software (Becton Dickinson). Fluorescence data were collected by using 488-nm excitation from a 15-mW air-cooled argon-ion laser. The emission was collected through a 530 ± 30-nm band-pass

filter (FL1-H). In addition, forward-light scatter (FSC-H) and side-light scatter (SSC-H) data were collected for each sample. The mean fluorescence uptake was defined as the number of the events multiplied by the geometric mean of the channel number.

Monitoring gene transfer in vivo

Tumors were induced by subcutaneous injection of 1×10^6 of either EMT6 or C26 cells in 6 week-old BALB/c mice (two mice for each cell line, two tumors/mouse). Ten-microgram DNA (1 μg/μL) of pGL3-control with NBs (15 μL) and saline (5 μL) were injected intratumorly for a total volume of 30 μL (day 0). The tumor was immersed into water and exposed to US at 3.0 W/cm^2 for 60 s. At day 1 and day 2, mice were anesthetized with isoflurane, subsequently received i.p. injection with luciferin (150 μg/g body weight) and were placed on the *in-vivo* imaging system. The bioluminescence signals were monitored using an IVIS100 (Xenogen Corp., Alameda, CA, USA).

Bioluminescence intensity and tumor volume

In-vivo studies were performed in accordance with the Tohoku University ethical guidelines. In this study, 11 BALB/c mice (8- to 10-week-old) were used. Tumors were induced by subcutaneous injection of 0.25×10^6/100 μL/site to 1×10^6/100 μL/site of EMT6-luc cells into both flanks (two tumors/mouse). The intensity and volume were measured from two to 23 days after inoculation. Each mouse was anesthetized with isoflurane and subsequently received i.p. injection with luciferin (150 μg/g body weight), and placed on the *in-vivo* imaging system to measure the bioluminescence signals. The tumor volume was measured with a caliper and calculated according to the formula $(\pi/6) \times (\text{width})^2 \times (\text{length})$.

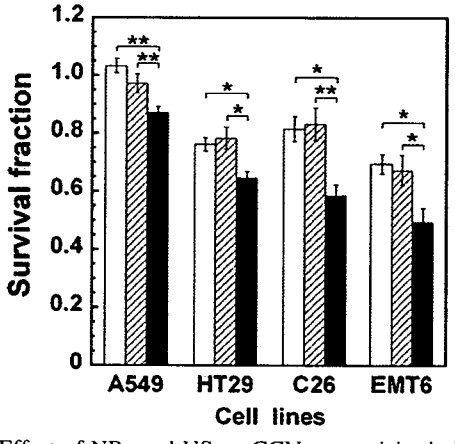

Fig. 1. Effect of NBs and US on GCV cytotoxicity in HSV*tk*-expressing cancer cells. Survival fractions were measured by MTT assay. Table 1 shows the number of samples used in Fig. 1. Each experiment consisted of six to 15 samples receiving US + NB + GCV with HSV*tk* (or Mock) and six to 15 control samples receiving US and NB. For each experiment, the mean % of treated samples was divided by the mean % of control samples to give a survival fraction. The mean of six to 15 survival fractions was calculated for each condition. □: US + NB + GCV; ▨: Mock + US + NB + GCV, ■: HSV*tk* + US + NB + GCV. A549 at day five with 5 μg/mL GCV, HT29 at day four with 10 μg/mL GCV, C26 examined at day three with 100 μg/mL GCV and EMT6 at day three with GCV 100 μg/mL). Ultrasound intensity was 1.3 W/cm^2. NB: lipid-micelle bubble. Bars represent the mean ± SEM. $*p < 0.05$; $**p < 0.01$.

Table 1. Number of samples per condition in Fig. 1.

	Control	□	▨	■
A549	6	6	6	6
HT29	6	6	6	6
C26	15	14	15	9
EMT6	12	10	9	12

A549: human lung adenocarcinoma cell, HT29; human colon carcinoma cell, C26: murine colon carcinoma cell, EMT6: murine mammary carcinoma cell. US: ultrasound, NB: nano/microbubbles, GCV: ganciclovir, Mock: pRS303 that does not have any transgene expressed, HSV*tk*: pGV24 vector in which the herpes simplex thymidine kinase (HSV*tk*) gene expression is driven by the ERBB2 promoter. □: US + NB + GCV, ▨: Mock + US + NB + GCV, ■: HSV*tk* + US + NB + GCV.

Therapeutic effect in vivo

Two types of experiments were conduced for low- and high-invasion tumors. Low-invasion case (subcutaneous tumor): SCID mice received subcutaneous injec-

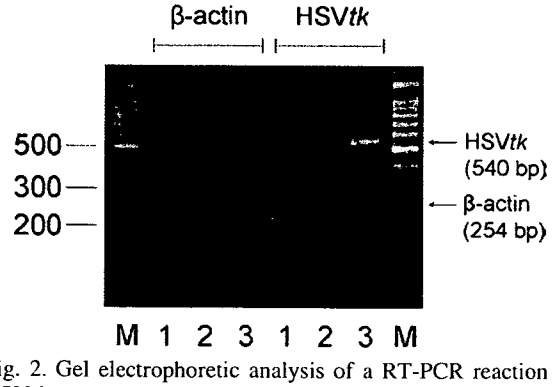

Fig. 2. Gel electrophoretic analysis of a RT-PCR reaction of HSV*tk* gene expressed in A549 cells induced by NBs and US. NB: lipid-micelle bubble. Lane M: 100-bp size ladder. Lane 1: cell alone. Lane 2: Mock + US + NB. Lane 3: HSV*tk* + US + NB. Total RNA was extracted from the cultures (pool of 6 wells) at 24 h after transfection, reverse-transcribed and amplified. The HSV*tk*-amplified fragment is 540 bp. The housekeeping gene, β-actin was 254 kb. This is a representative example from two separate experiments.

tions of 1 × 10^6/100 μL/site HT29-luc cells on each flank site on day 0 (2 tumors/mouse; 2 mice for control and mock groups, 3 mice for HSV*tk* group). The injection site was detectable more than three days after the injection because the skin color was changed. In addition, the site was given an India ink tattoo temporally. On days three, six, and nine, a total volume of 30 μL including 10 μL pHSV*tk* (1 μg/μg) (or pMock (1 μg/μg)) with 15 μL of NBs and 5 μL of saline was injected into the tumor site and the tumor was sonicated at 3.0 W/cm^2 for 60 s (2 tumors/mouse, 2 mice). On the same days, mice were imaged with the IVIS imaging system. From day four, GCV was administered i.p. to each mouse every day. High-invasion case (intramuscular tumor): 17 SCID mice received i.m. injection of 5 × 10^5/30 μL/site HT29-luc cells in each tibialis anterior muscle on day 0.

Every three days after day two, pHSV*tk* was injected into the tumor with US/NB method and GCV was injected i.p. five times per week for four weeks after day three. Eight control mice (3 mice [1 tumor/mouse] and 5 mice [2 tumors/mouse]) and three mice (1 tumor/mouse from HSV*tk* group) were culled on day 10 and the remaining six mice (3 mice in each group) were culled on day 30. On day 10, one or two tumors per each control mouse and one tumor for all mice in the treatment group were homogenized. On day 30, one tumor per mouse for all mice (3 mice in each group) was homogenized. All homogenized tumor samples were used to measure luciferase activity biochemically using a luciferase assay kit (Promega). Protein content was calculated using albumin standard curves (BCA Protein Assay Kit, Pierce, Rockford, IL, USA). Luciferase activity was converted to RLU/mg protein. Increase in the tissue temperature because of attenuation of US was ignored because the US frequency was 1 MHz and the depth of solid tumors (skin and muscle tumors) from the skin was <5 mm.

Statistical analysis

All measurements are expressed as mean ± SEM (standard error of mean). An overall difference between the groups was determined by one-way analysis of variance (ANOVA). Comparisons between two samples were made using Student's *t*-test. When the one-way

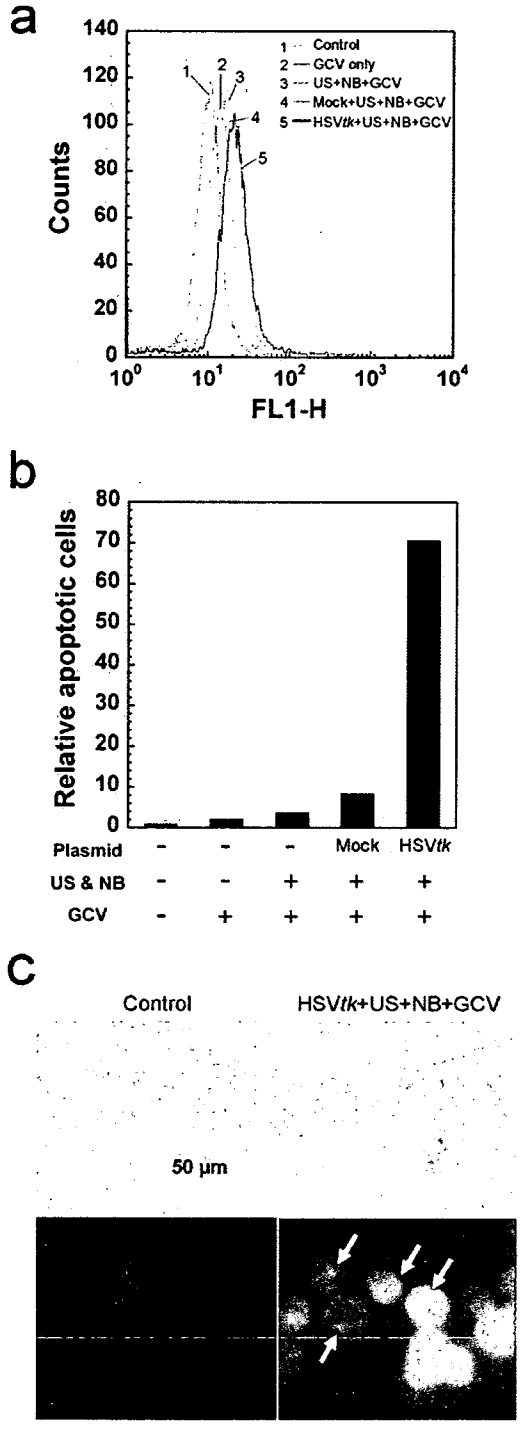

Fig. 3. Apoptosis analysis. (a) Histogram shows DNA fragmentation by TUNEL assay in A549 cells, measured at 48 h after the GCV treatment. GCV was 10 μg/mL. 1: Control (cell alone); 2: GCV alone; 3: US + NB + GCV; 4: Mock + US + NB + GCV; 5: HSV*tk* + US + NB + GCV. Cells were shifted to the higher fluorescence intensity values with increasing the number. (b) Number of TUNEL-positive cells obtained in Fig. 3a, expressed in bar chart. The emission was collected through a 530 ± 30-nm band-pass filter (FL1-H). The mean fluorescence uptake was defined as the number of the events multiplied by the geometric mean of the channel number, which was normalized with that of control cells alone. (c) Apoptosis in A549 cells was investigated by DAPI staining morphologically. A549 cells was incubated in the presence of GCV (10 μg/mL) for 24 h after the treatment of US + NB + HSV*tk*. NB: lipid-micelle bubble.

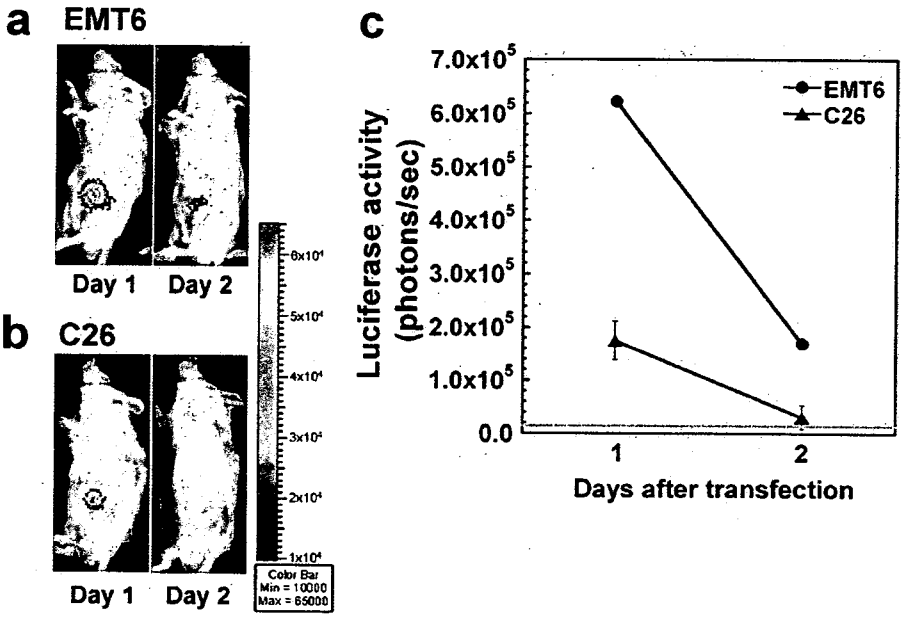

Fig. 4. Kinetics of luciferase gene expression in tumor-bearing BALB/c mice after gene transfection with US and NB. Two cell lines, EMT6 and C26, were used. Each cell line was injected into both flanks per mouse. Two mice were used for each cell line. (a, b) Representative images showing luciferase gene expression in the tumor of each cell on days 1 and 2. Color bar units represent photons/s/cm^2. (a) EMT6 cells. Gene expression was detected in only one flank. (b) C26 cells. Gene expression was detected in three flanks. (c) Luciferase activity with elapsed time. Background level (1.46×10^4 photons/s). Gene expression vanished in two days after the transfection by the US/NB method. Ultrasound intensity was 3.0 W/cm^2. NB: Optison. Bars represent the mean ± SEM.

ANOVA was significant and there were three samples, the differences between each group were estimated using the Tukey-Kramer test. The differences were considered to be significant at $p < 0.05$.

RESULTS

Gene transfer and GCV-mediated cytotoxicity in vitro

We first demonstrated that the combination of NBs with US could induce the sensitivity of different cell lines (A549, HT29, C26, EMT6) to killing by GCV *in vitro*. Because the sensitivity to GCV depends on the type of cells, the concentration of GCV and the assay day of cytotoxicity were varied for each cell line. MTT assay showed that exposure of US alone to cells (without NBs) did not induce cell damage (>0.95) (data not shown). Therefore, we compared HSV*tk* + US + NB + GCV with US +NB + GCV and Mock + US +NB + GCV. The MTT assay of four cell lines shows the significant cytotoxicity to GCV with HSV*tk* + US + NB + GCV compared with the control groups (Fig. 1). The sample numbers for each condition were shown in Table 1. HSV*tk* gene transfer was confirmed by RT-PCR (Fig. 2), where samples obtained under the same condition of Fig. 1 were analyzed. HSV*tk* + US + NB shows the single clear fragment (540 bp) compared with cell alone and Mock + US + NB, whereas the fragment (254 bp) of β-actin was observed for each condition.

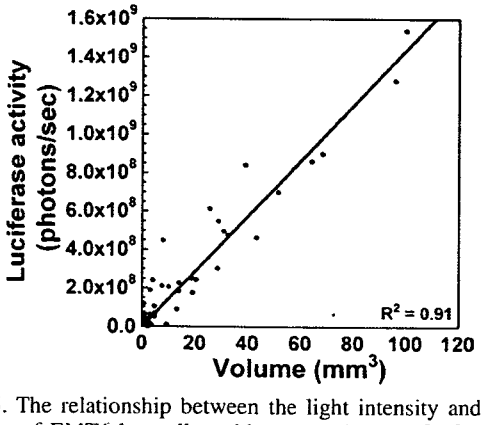

Fig. 5. The relationship between the light intensity and solid volume of EMT6-luc cells stably expressing the firefly luciferase gene. Cells were injected subcutaneously in mouse flanks (2 tumors/mouse). The number of mice and tumors was seven and 11, respectively. The intensity was measured from two to 23 days after inoculation. The volume was measured with a caliper. Tumor volume was calculated according to the formula $(\pi/6) \times (\text{width})^2 \times (\text{length})$.

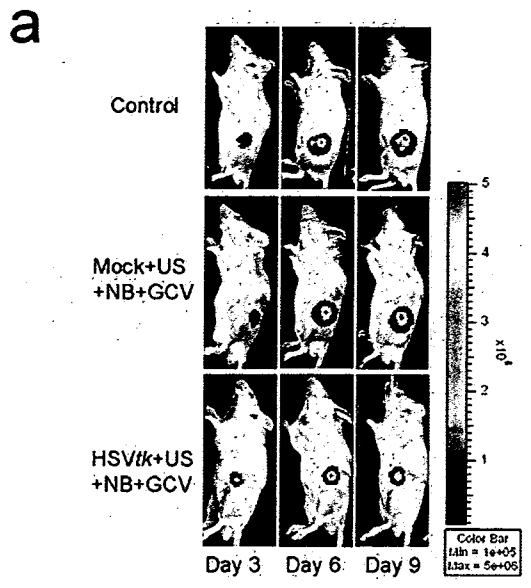

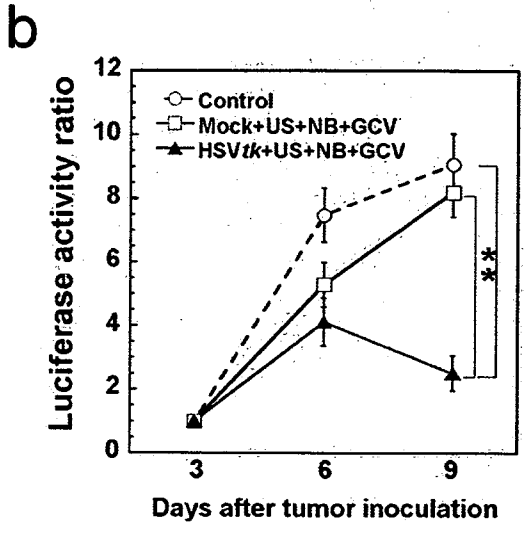

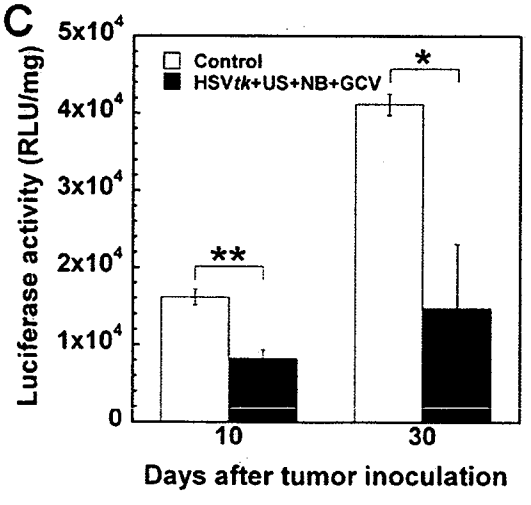

Apoptosis

We investigated whether the cytotoxicity was induced *via* apoptosis. Flow cytometry analysis of the TUNEL assay for A549 cells shows the curve in HSV*tk* + US + NB + GCV shifts largely to the right compared with other control groups, suggesting that dUTP labeled with biotin binds to DNA strand break (Fig. 3a). Figure 3b shows the histogram of Fig. 3a, indicating that the uptake of dUTP for HSV*tk* + US + NB + GCV is enhanced by a factor of 7 compared with Mock + US + NB + GCV. Because dUTP is also incorporated into DNA strands of necrotic cells, we stained A549 cells with DAPI staining and investigated the induction of apoptosis in the cells morphologically (Fig. 3c). As seen in Fig. 3c, apoptotic characteristics such as plasma membrane convolution, cytoplasmic blebbing, and nuclear condensation and fragmentation are observed; thus apoptosis is induced by the effect of HSV*tk*/GCV with the US/NB method.

Gene transfer in vivo*: Marker study*

The US/NB method induces a transient gene expression. First we investigated the kinetics of gene expression in tumor-bearing BALB/c mice by the US/NB method and determined the administration times by the US + NB. Two cell lines, EMT6 (Fig. 4a) and C26 (Fig. 4b), were used. Luciferase gene expression in these different solid tumors showed the same kinetics. The maximum luciferase activity was obtained at day one after transfection and reduced to the background level at day two (Fig. 4c). From these results, we delivered pHSV*tk* into tumor-bearing SCID mice by the US/NB method two to three times per week to maintain a high HSV*tk* gene expression level.

Fig. 6. Effect of GCV upon intratumoral HSV*tk* gene transfer with ultrasound and NB. (a, b) Data obtained with HT29-luc cells (1×10^6/100 μL of saline) injected subcutaneously into SCID mice. (a) Representative images showing bioluminescence in the tumors of each group on days three, six and nine. Color bar units represent photons/s/cm^2. (b) Bioluminescence was quantified at days three, six and nine. Statistical analysis was performed with the Tukey-Kramer test. Ultrasound intensity was 3.0 W/cm^2. NB: Optison. Bars represent the mean ± SEM; $^{**}p < 0.01$. (c) Tumors were induced by i.m. injection of HT29-luc cells (5×10^5/30 μL of saline) into each tibialis anterior muscle of SCID mice for each group on day zero, and from day three, GCV 40 (mg/kg) diluted in PBS was given daily. Tumors were removed and homogenized at 10 and 30 d. The luciferase activity was measured with a luminometer. Statistical analysis was performed by using Student's *t*-test. Ultrasound intensity was 3.0 W/cm^2. NB: Optison. Bars represent the mean ± SEM; $^*p < 0.05$, $^{**}p < 0.01$.

Bioluminescence intensity and tumor volume

We investigated the linearity between the bioluminescence intensity and the solid tumor volume. EMT6-luc cells were injected subcutaneously. The cells allowed us to measure the size of the tumor because the cells are relatively low invasive and the boundary of the generated solid tumor is identified relatively easily. The volume was measured with a caliper and the light intensity was obtained with the *in-vivo* imaging system. As seen in Fig. 5, the linearity between the bioluminescence intensity and the tumor volume was kept up to 100 mm^3 (the width of solid tumor was <6 mm). Therefore, tumors with a volume <100 mm^3 were analyzed with the *in-vivo* imaging system in the experiment.

Therapeutic effects in vivo

Based on Figs. 4 and 5, we investigated the antitumor effect of US/NB-mediated HSV*tk* gene transfer to HT29-luc bearing SCID mice for the first experiment. The cells were injected and grown subcutaneously. The tumors were transduced three days after tumor cell inoculation and gene transfer was repeated on days six and nine. Daily i.p. injection of GCV (40 mg/kg) was administered from day four. Figure 6a and b show that a very significant reduction in tumor volume in mice treated with HSV*tk*, US, NB and GCV compared with control groups indicate that the US/NB method has therapeutic effects.

In clinical practice, most tumors may not be distinguished clearly from normal tissue as they are infiltrated into normal tissue. In a second experiment, HT29-luc cells were injected into the TA muscle and the tumors treated by US/NB-mediated gene transfer and GCV. US/NB-mediated HSV*tk* gene transfer was performed every three days from day four and GCV (40 mg/kg) was administered five times per week. Bioluminescence of the tumors *in vivo*, as well as enzymatic activity on biopsies, was measured (Fig. 6c). Luciferase activity measured biochemically on day 10 shows a statistical difference in tumor burden between control and HSV*tk* + US + NB + GCV. Furthermore, there was a statistical difference in tumor burden on day 30, with mice treated with HSV*tk* + US + NB + GCV, showing a 4 times reduction in tumor burden compared with control (Fig. 6c). During the course of these experiments, no weight reduction was observed in treated and untreated mice. Altogether, these results demonstrate the potential of HSV*tk* + US + NB + GCV treatment.

DISCUSSION

The concept of the molecular delivery method using US and NB is to induce a transient membrane permeability of cells, followed by the entry of exogenous molecules into the cells. It has been suggested that the impulsive pressures generated by either the collapse of NBs or cavitation bubbles created by the collapse of NBs are able to induce a transient permeabilization of cells, followed by the entry of exogenous molecules into cells. Gene or oligodeoxynucleotide transfer using NB and US has already been reported (Kodama et al. 2005, 2006a, 2006b; Takahashi et al. 2007), but in this manuscript we demonstrate that this technology can be applied successfully to cancer gene therapy. *In-vitro* US/NB-mediated transfer of the HSV*tk* gene (Fig. 2) and incubation of the transduced cells with GCV leads to reduced cell survival (Fig. 1). This DNA-dependent cell kill was achieved through apoptosis (Fig. 3), as expected from the well-established mode of action of HSV*tk*/GCV (Freeman et al. 1993; Hamel et al. 1996; Wallace et al. 1996; Yoon et al. 1999).

In the present *in-vivo* study, we evaluated the *in-vivo* cytotoxicity by US/NB-mediated gene transfer by bioluminescence. The linearity between the intensity of bioluminescence and the tumor volume was kept up to a volume of 100 mm^3 (the width was <6 mm) (Fig. 5), where tumor volume was calculated according to the formula $(\pi/6) \times (\text{width})^2 \times (\text{length})$. In general, tumor size correlates closely with light intensity (Mendel et al. 2003; Soling et al. 2004). In agreement with our observations, Soling et al. (2004) reported that tumor size is not correlated with light intensity when the tumor becomes large (>12–15 mm in diameter) based on the same equation. In fact, in our recent studies, we have found that bioluminescence measurement collected using the IVIS imaging system showed a great correlation between mean bioluminescence and mean 3D tumor volume quantified using high frequency ultrasound imaging system (data not shown).

In-vivo gene expression was detectable 24 h after transfection and was dramatically reduced 48 h later (Fig. 4), highlighting the transient nature of US/NB-mediated gene transfer. This kinetics is in sharp contrast with adenovirus-mediated (Groot-Wassink et al. 2002, 2004) or nonviral gene transfer (Harada-Shiba et al. 2002; Yoshino et al. 2006), which usually lead to a maximal level of expression 48 h after transduction and can last several days at least. The transient nature of US/NB-mediated gene delivery has implications when applied in the context of pro-drug activation therapy: gene delivery must be repeated and the pro-drug must be provided shortly after transduction. This transient expression is likely to be the result of rapid plasmid DNA degradation.

In many *in-vivo* experiments, solid tumors are induced subcutaneously and used as therapeutic targets. However, therapeutic effects need to be considered using tumors infiltrated into normal tissues. In the present

experiment, we provided data demonstrating therapeutic effects of US/NB-mediated gene transfer for two types of tumors. One was subcutaneous (low-invasive) and the other was i.m. tumors (high-invasive). Figure 6 clearly shows the efficacy of the treatment with low-invasive and (Fig. 6a and b) high-invasive tumors (Fig. 6c) by US/NB-mediated gene transfer.

Considering the efficacy of the current version of NBs presented in this report and the potential for chemical modifications of the shell material (Li et al. 2003; Wang et al. 2005), and for incorporation of specific ligands in the shell membrane to enhance the tissue-specificity against the target site (Lindner 2004), the system associating NB, DNA and US could provide an alternative option to viral cancer gene therapy.

Acknowledgments—We thank Kiyoe Konno and Sachiko Horie for technical assistance. This work was supported in part by the Encouraging Development of Strategic Research Center, Special Coordination Funds for Promoting Science and Technology, MEXT (Ministry of Education, Culture, Sports, Science and Technology). T.K. acknowledges Grant-in-Aid for Scientific Research (B) (17300168), Grants-in-Aid for Exploratory Research (18650140), Grant-in-Aid for Scientific Research on Priority Area, MEXT (17012002, 18014002) and Research on Advanced Medical Technology, The Ministry of Health Labour and Welfare (H17-nano-006 and H19-nano-010). G.V. acknowledges program and projects grants from Cancer Research UK, and INSERM and Institut National du Cancer (INCa). GCV was donated from F. Hoffman-La Roche Ltd., Basel, Switzerland.

REFERENCES

Ammi AY, Cleveland RO, Mamou J, Wang GI, Bridal SL, O'Brien WD. Ultrasonic contrast agent shell rupture detected by inertial cavitation and rebound signals. IEEE Trans Ultrason Ferroelectr Freq Control 2006;53:126–136.

Aoi A, Konno K, Shinohara F, Mori S, Vassaux G, Kodama T. Effects of anti-cancer drug of cisplatin using nanobubbles and ultrasound. Ultrasound Med Biol 2006;32:280.

Chen SH, Chen XH, Wang Y, Kosai K, Finegold MJ, Rich SS, Woo SL. Combination gene therapy for liver metastasis of colon carcinoma *in vivo*. Proc Natl Acad Sci U S A 1995;92:2577–2581.

Chomas JE, Dayton P, Allen J, Morgan K, Ferrara KW. Mechanisms of contrast agent destruction. IEEE Trans Ultrason Ferroelectr Freq Control 2001;48:232–248.

Fillat C, Carrio M, Cascante A, Sangro B. Suicide gene therapy mediated by the Herpes Simplex virus thymidine kinase gene/Ganciclovir system: Fifteen years of application. Curr Gene Ther 2003;3:13–26.

Freeman SM, Abboud CN, Whartenby KA, Packman CH, Koeplin DS, Moolten FL, Abraham GN. The "bystander effect": Tumor regression when a fraction of the tumor mass is genetically modified. Cancer Res 1993;53:5274–5283.

Groot-Wassink T, Aboagye EO, Glaser M, Lemoine NR, Vassaux G. Adenovirus biodistribution and noninvasive imaging of gene expression *in vivo* by positron emission tomography using human sodium/iodide symporter as reporter gene. Hum Gene Ther 2002; 13:1723–1735.

Groot-Wassink T, Aboagye EO, Wang Y, Lemoine NR, Keith WN, Vassaux G. Noninvasive imaging of the transcriptional activities of human telomerase promoter fragments in mice. Cancer Res 2004; 64:4906–4911.

Hamel W, Magnelli L, Chiarugi VP, Israel MA. Herpes simplex virus thymidine kinase/ganciclovir-mediated apoptotic death of bystander cells. Cancer Res 1996;56:2697–2702.

Harada-Shiba M, Yamauchi K, Harada A, Takamisawa I, Shimokado K, Kataoka K. Polyion complex micelles as vectors in gene therapy—Pharmacokinetics and *in vivo* gene transfer. Gene Ther 2002; 9:407–414.

Harvey CJ, Blomley MJ, Eckersley RJ, Cosgrove DO. Developments in ultrasound contrast media. Eur Radiol 2001;11:675–689.

Keller PM, Fyfe JA, Beauchamp L, Lubbers CM, Furman PA, Schaeffer HJ, Elion GB. Enzymatic phosphorylation of acyclic nucleoside analogs and correlations with antiherpetic activities. Biochem Pharmacol 1981;30:3071–3077.

Kodama T, Aoi A, Vassaux G, Mori S, Morikawa H, Koshiyama K, Yano T, Fujikawa S, Tomita Y. A non-invasive tissue-specific molecular delivery method of cancer gene therapy. Minim Invasive Ther Allied Technol 2006a;15:226–229.

Kodama T, Doukas AG, Hamblin MR. Delivery of ribosome-inactivating protein toxin into cancer cells with shock waves. Cancer Lett 2003;189:69–75.

Kodama T, Tan PH, Offiah I, Partridge T, Cook T, George AJ, Blomley MJ. Delivery of oligodeoxynucleotides into human saphenous veins and the adjunct effect of ultrasound and microbubbles. Ultrasound Med Biol 2005;31:1683–1691.

Kodama T, Tomita Y, Koshiyama K, Blomley MJ. Transfection effect of microbubbles on cells in superposed ultrasound waves and behavior of cavitation bubble. Ultrasound Med Biol 2006b;32: 905–914.

Li T, Tachibana K, Kuroki M, Kuroki M. Gene transfer with echo-enhanced contrast agents: Comparison between Albunex, Optison, and Levovist in mice—Initial results. Radiology 2003;229:423–428.

Lindner JR. Microbubbles in medical imaging: current applications and future directions. Nat Rev Drug Discov 2004;3:527–532.

Martinico SC, Jezzard S, Sturt NJ, Michils G, Tejpar S, Phillips RK, Vassaux G. Assessment of endostatin gene therapy for familial adenomatous polyposis-related desmoid tumors. Cancer Res 2006; 66:8233–8240.

McCulloch M, Gresser C, Moos S, Odabashian J, Jasper S, Bednarz J, Burgess P, Carney D, Moore V, Sisk E, Waggoner A, Witt S, Adams D. I. Ultrasound contrast physics: A series on contrast echocardiography, article 3. J Am Soc Echocardiogr 2000;13:959–967.

Mendel DB, Laird AD, Xin X, Louie SG, Christensen JG, Li G, Schreck RE, Abrams TJ, Ngai TJ, Lee LB, Murray LJ, Carver J, Chan E, Moss KG, Haznedar JO, Sukbuntherng J, Blake RA, Sun L, Tang C, Miller T, Shirazian S, McMahon G, Cherrington JM. In vivo antitumor activity of SU11248, a novel tyrosine kinase inhibitor targeting vascular endothelial growth factor and platelet-derived growth factor receptors: Determination of a pharmacokinetic/pharmacodynamic relationship. Clin Cancer Res 2003;9:327–337.

Mesnil M, Yamasaki H. Bystander effect in herpes simplex virus-thymidine kinase/ganciclovir cancer gene therapy: Role of gap-junctional intercellular communication. Cancer Res 2000;60:3989–3999.

Oliver S, Bubley G, Crumpacker C. Inhibition of HSV-transformed murine cells by nucleoside analogs, 2′-NDG and 2′-nor-cGMP: Mechanisms of inhibition and reversal by exogenous nucleosides. Virology 1985;145:84–93.

Pitt WG, Husseini GA, Staples BJ. Ultrasonic drug delivery—A general review. Expert Opin Drug Deliv 2004;1:37–56.

Soling A, Theiss C, Jungmichel S, Rainov NG. A dual function fusion protein of Herpes simplex virus type 1 thymidine kinase and firefly luciferase for noninvasive *in vivo* imaging of gene therapy in malignant glioma. Genet Vaccines Ther 2004;2:7.

Takahashi M, Kido K, Aoi A, Furukawa H, Ono M, Kodama T. Spinal gene transfer using ultrasound and microbubbles. J Control Release 2007;117:267–272.

Vassaux G, Hurst HC, Lemoine NR. Insulation of a conditionally expressed transgene in an adenoviral vector. Gene Ther 1999;6: 1192–1197.

Vassaux G, Martin-Duque P. Use of suicide genes for cancer gene therapy: Study of the different approaches. Expert Opin Biol Ther 2004;4:519–530.

Wallace H, Clarke AR, Harrison DJ, Hooper ML, Bishop JO. Ganciclovir-induced ablation non-proliferating thyrocytes expressing herpesvirus thymidine kinase occurs by p53-independent apoptosis. Oncogene 1996;13:55–61.

Wang X, Liang HD, Dong B, Lu QL, Blomley MJ. Gene transfer with microbubble ultrasound and plasmid DNA into skeletal muscle of mice: Comparison between commercially available microbubble contrast agents. Radiology 2005;237:224–229.

Wu J, Tong J. Experimental study of stability of a contrast agent in an ultrasound field. Ultrasound Med Biol 1998;24:257–265.

Yoon SS, Carroll NM, Chiocca EA, Tanabe KK. Influence of p53 on herpes simplex virus type 1 vectors for cancer gene therapy. J Gastrointest Surg 1999;3:34–48.

Yoshino H, Hashizume K, Kobayashi E. Naked plasmid DNA transfer to the porcine liver using rapid injection with large volume. Gene Ther 2006;13:1696–1702.

解説

ナノ・マイクロバブルと超音波を用いた分子導入システムの開発とがん治療への応用

Development of Molecular Delivery System Using Nano/Microbubbles and Ultrasound: Application to Cancer Therapy

小玉　哲也
Tetsuya KODAMA

◎1992年3月東北大学大学院工学研究科機械工学専攻修了，工学博士．同年オックスフォード大学物理化学研究所客員研究員，1993年ロンドン大学セント・トーマス病院医療物理学科客員研究員，1994年東北大学流体科学研究所助手，1998年ハーバード大学医学部皮膚科講師，2000年ハーバード大学医学部内科研究員，2002年ロンドン大学インペリアルカレッジ医学部画像科学学科研究員を経て，現職
◎研究・専門テーマは，ナノメディシン，分子デリバリーシステム，がん治療，気泡力学
◎正員，東北大学准教授　先進医工学研究機構
（〒980-8575　仙台市青葉区星陵町2-1／E-mail: kodama@tubero.tohoku.ac.jp）

1. はじめに

1981年以来，日本の死因の第一位は「がん」になった．2005年のがんの死亡数は32万人で，総死亡数の30%に相当する．2015年には89万人ががんに罹患すると推定され，この値は2005年現在の山梨県民数88万人に匹敵する．2007年度の厚生労働省の対がん予算は212億円に増額され，予算額に見合った研究成果を挙げ，がんに苦しむ患者を早急に救うことが求められる[1]．現在，外科療法，化学療法，放射線療法が三大療法とされ，近年では第四の療法として免疫療法が注目されている．

がんの根治の難しさのひとつは，がん転移に対して有効な抑制法が見出されていないことである．腫瘍であると判断された場合には，すでに10億個以上のがん細胞がぶどう程度の大きさになっており，この時点でがん細胞の一部は分裂してほかの部位に転移している可能性が高い．上記の四つの手法に代わる新規ながん治療法の開発を目指すには，転移性がんに着目するのではなく，限局して増殖するがんを対象に，局所投与を基本とする分子導入法の開発が有効である．

いっぽう，がんの早期診断は治療成績に反映される．超音波造影剤（ナノ・マイクロバブル）はシェル構造からなる直径10μm以下のガスバブル（大概は2〜4μm）である．微小循環中で赤血球（成人男性では平均直径7.5μm）と類似した挙動を示すことから，血液プールや微小循環レベルでの血流を評価するために使用されてきた．非粘性，非圧縮性流体内で振動する気泡の固有振動数の関係式[2]から直径2〜4μmの固有振動数を求めると，1.6〜3.2MHzとなり，偶然にも臨床でよく使用される超音波プローブの振動数3.5MHzに近似する．この偶然性のために，バブルの固有振動から得られるハーモニック信号を処理することで超音波画像の画質と診断技術が改善され，超音波診断学に新しい研究分野が展開されている．

本稿では，ナノ・マイクロバブルと超音波を利用した新しい分子導入システムと，このシステムのがん治療への応用に関して解説する．

2. バブルと超音波を用いた分子導入法

超音波造影剤を超音波で破壊させて，遺伝子や抗癌剤などの外来分子を細胞に導入し疾患治療に応用する試みは1996年頃から報告され，現在では心臓血管疾患，炎症性疾患，がん治療への応用が期待されている．この手法は非侵襲的であり，ウイルスによる外来分子導入の際に問題となる免疫原性[注1]はなく，また体内のバブルの動きを体外からモニタできることから組織選択的に外来分子を導入できる利点がある．しかしながら，この手法の問題点は分子導入効率の低さであり，導入手法に工夫が必要だ．

対象とする細胞の種類にもよるが，この手法による分子導入効率は，細胞実験でせいぜい20〜30%が限度である．動物実験ではさらに低くなる．バブル崩壊が分子導入の機

（注1）免疫原性　一般に，「抗原性」とは，ある物質が抗体と反応することができる性質．「免疫原性」とは，その物質と特異的に反応することができる抗体を生体内に誘起することができる性質と考えられている．したがって，ウイルスを使用した遺伝子導入ではウイルス自体が抗原となって，体内にこれに対する抗体が生産される．ウイルス導入法は効率的ではあるが，不必要な免疫を誘導するうえ，標的組織以外に感染して死亡事故や白血病の発生につながるなど，安全性に問題を抱えている．

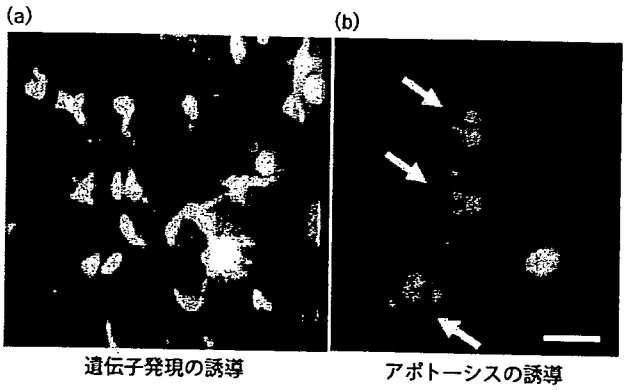

図1　分子導入にともなう生体反応
(a) マウス結腸がん(Colon26) 細胞にオワンクラゲ由来改変型緑色蛍光タンパク質を発現するプラスミドを導入し，24時間後に蛍光顕微鏡下で観察する．
(b) マウス結腸がん(Colon26) 細胞に抗癌剤であるシスプラチンを導入し，DAPIで染色後，蛍光顕微鏡で観察．矢印は細胞核の分断と断片化を示す．白線は10μmの長さを示す．

序に関与すると指摘されれば，だれしもバブルの直径から概算できる固有振動数でバブルを強制的に振動させればよいと推測はできる．しかし，分子導入に要求される超音波の振動数は，バブルの固有振動数より低い1MHz程度が導入に適している．なぜこの周波数なのかという解答はまだ得ていないが，この周波数を固定し，他の超音波条件(パルスモード，パルス数，デューティ比，出力，圧力の空間分布等) を最適化することで，細胞に外来分子を導入することが可能になる．図1(a) はマウス結腸がん(Colon26) 細胞にオワンクラゲ由来改変型緑色蛍光タンパク質を発現するプラスミド(注2)を導入し，24時間後に，蛍光顕微鏡で遺伝子の発現を観察した例である．図1(b) はColon26細胞に抗がん剤であるシスプラチンを導入し，抗腫瘍効果の検証を行った実験である．導入24時間後に，細胞核を染める色素(DAPI) で染色し，蛍光顕微鏡で観察すると，アポトーシス(Apoptosis)(注3)に特徴的な核の分断と断片化が認められる．本手法のような物理的な分子導入法でも，細胞の生命機能を調整してアポトーシスを誘導できることが示されており，将来の新しい抗がん剤の開発が期待できる．

本手法ががん遺伝子治療に応用できるかどうか，実際に治療用遺伝子をがん細胞に導入して，その効果を検討してみよう．図2ではルシフェラーゼ発現ヒト大腸がん(HT29-luc) 細胞で固形腫瘍をマウス側腹に作製し，つぎに治療用遺伝子である単純ヘルペスチミジンキナーゼ遺伝子[Herpes Simplex Virus-thymidine kinase(HSV*tk*) gene] を2～3日間隔で導入した後，毎日ガンシクロヴィル(GCV) を静脈注射して抗腫瘍効果の検証を行った例である(注4)．同一個体での抗腫瘍効果を生体発光イメージング法で観察する．腫瘍作製後9日目には抗腫瘍効果が顕著に観察されており，がん遺伝子治療への応用の可能性が示されている[3]．

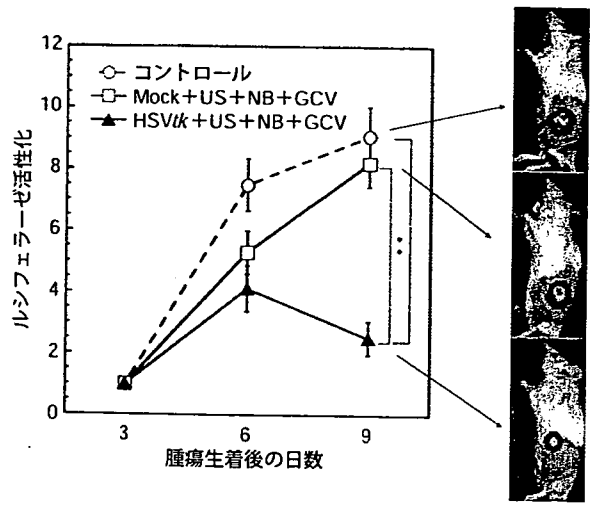

図2　単純ヘルペスチミジンカイネース(HSV*tk*) とガンシクロビル(GCV) を組み合わせた自殺遺伝子療法
MockはHSV*tk*プラスミドDNAからHSV*tk*遺伝子配列を取り除いたプラスミドDNAである．Mockのデータはプラスミド DNAの細胞への導入自体が細胞毒性を誘起しないことを示すために必要である．NB: ナノマイクロバブル，US: 超音波．$P<0.01$ (**)．

3. ナノバブルと臨床 意味のあるがん

80歳半ばを過ぎた私の伯母は，会うたびに「研究成果は上がっているか」，と質問をしてくる．「まだ」と返事をすると「税金を使って何をしているんだ」と叱咤される．大学に席を置く者にとって，また医工学研究を行っている者にとっては，研究成果は最終的には臨床に応用されるべきであり，しかも短期間に成果を挙げないと，この伯母を代表とする国民の支持は得られない．研究の方向性や進ちょく度は臨床応用に向かうタイムスケジュールの中で調整する必要がある．

ナノというサイズは，がん組織内に網羅された新しい血管ネットワーク(血管新生) から漏出するに必要な粒子の直径として求められる値である．血管新生は通常の血管と異なり，直径200nm以下の粒子が血管壁から漏出・滞留する，いわゆるEPR効果(Enhanced Permeability and Retention Effect) が確認されている．もしこのサイズ以下のバブルが注射された場合にはEPR効果で漏出・滞留するバブルを超音波画像として認知できるはずで，腫瘍新生

(注2) プラスミド　小さなDNA分子で一般には環状である．蛍光タンパク質や治療用タンパク質を細胞内で作成するには，これらのタンパク質の生成を誘導する遺伝子をプラスミドのDNA配列に組み入れる必要がある．
(注3) アポトーシス　細胞には「自ら自滅するように指令する遺伝子」が組み込まれており，この働きで細胞が自殺死することを「アポトーシス」という．これに対し，血行不良，外傷などによって起こる細胞死は，ネクローシスまたは壊死と呼ばれ，これと区別される．生体内では，がん化した細胞のほとんどは，アポトーシスによって取り除かれ続けており，これにより，ほとんどの腫瘍の成長は未然に防がれていることが知られている．細胞の形態変化，核の凝縮・分断化，染色体の断片化，細胞膜の脂質の局在でアポトーシスの発生を判断する．
(注4) 自殺遺伝子療法　本来，ほ乳動物に存在しない微生物由来の代謝酵素遺伝子を導入し，その酵素で活性化されるプロドラッグを用いることにより細胞障害性を誘導する方法．HSV*tk*遺伝子と抗ウイルス剤GCVを用いた方法は自殺遺伝子治療のひとつ．

表1 局所投与が臨床的に有効ながん

腫瘍	投与法	理由	死亡数 2003年)	
			男性	女性
脳腫瘍	動注(内頚動脈)	他臓器への転移なし	833	624
肝がん	動注(肝動脈)	他臓器への転移がほとんどない. 肝内で広がって肝不全で死亡	23 376	10 713
膀胱がん	膀胱注入	浸潤しない 膀胱内再発率は,単発性で30〜40%,多発性は約70〜90%	3 719	1 693
卵巣がん	腹腔内投与	腹腔内投与	−	4 231

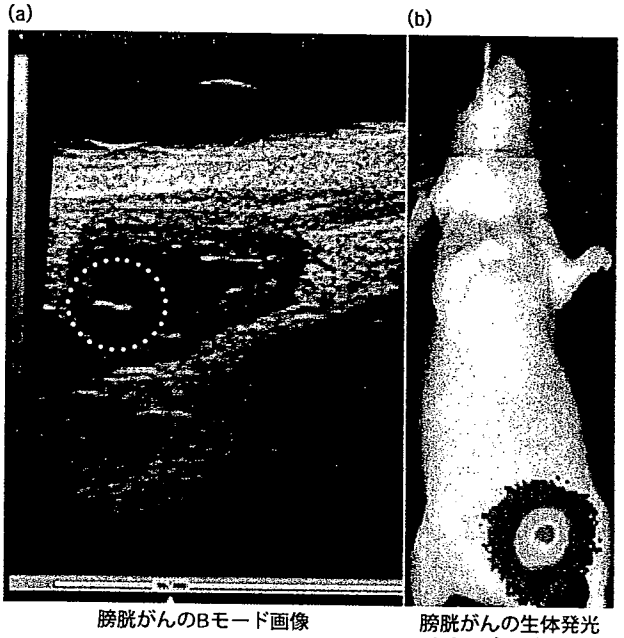

図3 マウス膀胱がんモデル
(a) 超音波画像で生着し増殖する膀胱がんを確認(破線円内).
(b) 超音波画像で確認した膀胱がんを生体発光イメージング法で体外から確認.

血管を標的とした新しい分子導入法の開発が可能になる.

薬剤を導入する方法には全身投与(静脈注射)と局所投与(動脈注射,腹腔内投与,膀胱内投与等)に大別される.分子送達率は全身投与より局所投与が1 000倍程度高い.局所投与と上記のEPR効果との相乗効果を考えると,本手法に適する「臨床的に意味のあるがん」は自ずと限定されてしまう.ここでいう「臨床的に意味のあるがん」とは,本手法の有効性に期待でき,かつ,既存の治療方法では治療効果に限度があり,新しい治療法の開発が望まれる「がん」として定義する.表1は,この「がん」である.膀胱がんは大きく分けて表在性膀胱がん,膀胱上皮内がん,浸潤性膀胱がんの3種類に分類されるが,ほとんどの場合は表在性膀胱がんであり,再発率は単発性で30〜40%,多発性の場合は約70〜90%である.現在,国立がんセンター東病院(松村保広部長)と臨床試験を念頭に表在性膀胱がんを対象に共同研究を行っている.局所投与を基本としており,この場合はEPR効果との相乗効果は考えていない.図3は表在性膀胱がんモデルの例であり,膀胱がん生着後21日目の結果である.図3(a)はマウス膀胱内で作成されたルシフェラーゼ発現膀胱がんの超音波画像,図3(b)はその生体発光イメージング画像である.核酸(プラスミドやsiRNA等)や抗がん剤を含めた治療用分子を使い抗腫瘍効果を検証しており,今度,伯母に会ったら「成果はあがっている」と返答する予定である.

4. 分子の導入メカニズム

バブルと超音波を使った分子導入法はバブル崩壊で発生する衝撃圧と,バブル崩壊後に誘起されるキャビテーション気泡の衝撃圧とを利用して,細胞膜に一過性の構造変化を誘導して外来分子を細胞質や細胞核に導入することを基本概念としている(図4).衝撃圧には液体ジェットや衝撃波などが含まれるが,いずれにせよ,重畳した衝撃圧が細胞膜に作用しているに違いない.

いま,バブルが崩壊して球状のキャビテーション気泡が発生したと仮定しよう.キャビテーション気泡の急激な半径方向の運動は壁面近傍の流体を圧縮・駆動する.この圧縮された液体には圧力波が形成される.圧力波の非線形波面は衝撃波面へと変形しながら,圧力波は衝撃波として伝播する.この衝撃波は気泡周囲の細胞と干渉して細胞膜の

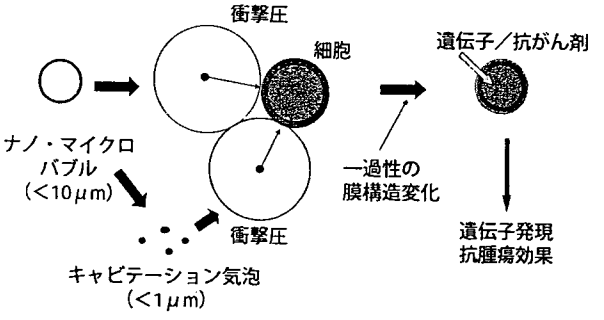

図4 分子導入のメカニズム

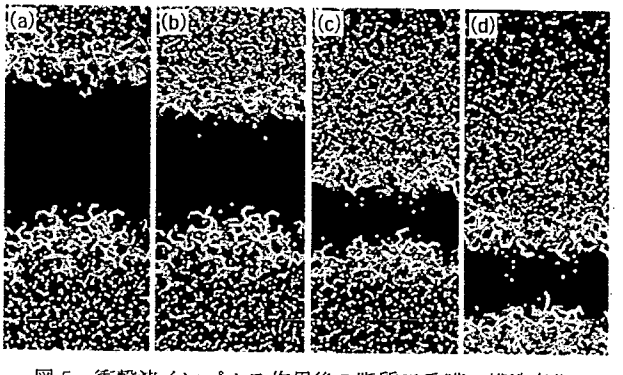

図5 衝撃波インパルス作用後の脂質二重膜の構造変化
衝撃波インパルスの作用を受けた脂質二重膜の変形を分子動力学シミュレーションで解析する.水分子を青色で表記し,アシル鎖は水分子の動きを理解しやすいように色付けしていない.(a) 平衡状態,(b) 0.15ps後には球水基に水分子が移動し始める,(c) 0.30ps,(d) 0.45ps. 平衡状態にあっても,水分子は球水基に存在する[9].

透過性を促し，外来分子の細胞内部への拡散に寄与するものと考えられる．衝撃波を分子動力学シミュレーションで記述すること自体，チャレンジングな課題であるが，いま衝撃波を衝撃波インパルス（衝撃波圧力の時間履歴を時間で積分した値）と定義して，細胞膜に衝撃波インパルスが作用したと仮定しよう．細胞膜は脂質とタンパク質からなる約5nmの薄い二重膜である．ここでは脂質の主成分のひとつであるジパルミトイルホスファチジルコリン（DPPC）で構成された脂質二重膜が水に浮かんだ状態に衝撃波インパルスが作用したと考える．図5は衝撃波インパルスが上から下に向かって作用した場合のシミュレーションである．衝撃波インパルス作用後に脂質二重膜は大きく変形し，脂質外側にある水分子は脂質内に移動する[4]．水分子が強制的に脂質内に導入された場合は，やがて脂質膜に水孔が形成されることが示されており，外来分子はこの水孔から細胞内に導入されるのではと考えられる．

5. 治療性標的バブルと診断

生あるもの，血球細胞であれ，血管組織であれ，体内への侵入者に対して，あるいは自己の体調不調や活性化について何らかのシグナルを周囲に発信する．たとえば，がん細胞が転移して増殖する際には血管を新生する．この新生血管の内皮には周囲へのシグナルとしてVEGFR-2をはじめとする多くの腫瘍マーカ（リセプタ）が発現する．したがって，このマーカに対するリガンドをバブルのシェルに組み込むことで，血流に沿って流れ行くバブルは，リセプタ・リガンド反応でこの発現部位に捕獲されると期待できる．現在，われわれは図6に示すような治療用分子を内包し，かつシェル表面には疾患部位を標的とする分子を組み入れたさまざまな治療性・標的バブルを作成中である．これにより，標的部位への治療分子の導入効率の改善を目指している．

現在のCTやMRIでは1cm以下の組織の塊が「がん」であると判断することは難しい．バブルの体内循環は超音波画像でよく見える．このバブルの軌跡で描写される三次元画像を構築したらどのように見えるだろうか？　血管新生は通常の血管と異なり，湾曲し，血管径が不ぞろいであるなど特徴的である．この特徴がバブルの軌跡で得られる血管構造から判断できれば，新しいがんの早期診断法の開発が可能だ．現在，われわれはこの視点に立って研究を進めており，興味あるデータを収得し始めた．

昨今のIT技術の進展は目覚しい．この技術を使えば，地域間・国家間を越えた治療法・診断法の開発ができ，医療格差を是正できる可能性がある．それには，国家間を越えて臨床現場で得られる診断情報をネットワークで連結して，大量の医療情報をスーパコンピュータで処理することが必要だ．私が所属する研究室は東北大学医学部星陵キャンパスにある．現在，直線距離で3.5km離れた東北大学片平キャンパスの流体科学研究所設置のスーパコンピュータに超音波画像情報を転送して，上記のモデルを実現しようと試みている．2007年6月に南アフリカKwazulu-Natal大学の副学長が本学を訪問された．ホストコンピュータをヨーロッパに置くことで時差なしの医療診断ができるのではと申し上げた．大変興味を持たれたようで，後日，東京の南アフリカ大使館からパーティの招待状が届いた．粋なことをすると感じ入っていたら，大学関係者のすべてに送っていたようで，心の機微を理解した外交関係を行うものだ，とさらに感心が深まった．

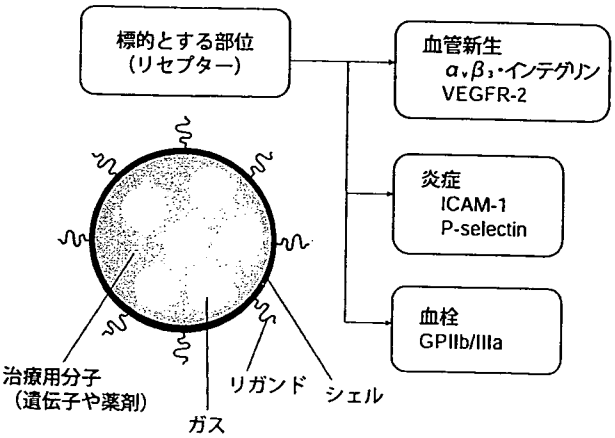

図6　治療性と標的性の高いバブルの作成

6. おわりに

がん治療法の開発を研究目標に掲げる者として，がん患者数ゼロ達成が最大の目標である．さまざまな治療法や薬剤が開発されても，治療成果はあがらないのが現状である．これまで海外で生活をする機会があったが，帰宅後に自分の服にタバコの臭いを感じられた日数が年間を通していちばん少なかった国はアメリカだった気がする．タバコだけが「がん」の原因ではないが，自らが，あるいは社会・国家が率先して「がん」発生因子の軽減に真摯に取り組まないど「がん」を克服できないのでは考えている．キャビテーション気泡による繰り返しの衝撃圧の作用で，流体機械は材料損傷を受けてしまう．人間の体も精密な機械であり，常に外部刺激により分子レベルで損傷を受けており，限度を超えた刺激には修復しきれない．（社）日本機械学会会員数は40 000人であり，日本最大の学会である．人間の体という精密機械をもっとたいせつにする運動を広げることで，学会は別な角度から日本・世界に貢献できるのではないだろうか．

（原稿受付2007年8月30日）

●文　献
（1）がん研究振興財団，がんの統計'07，2007年版，（2007），6-22.
（2）Minnaert, M., On Musical Air Bubbles and the Sounds of Running Water, *Philosophical Magazine*, **16**-104（1933），235-248.
（3）Aoi, A., Watanabe, Y., Mori, S., Takahashi, M., Vassaux, G. and Kodama, T., Herpes Simplex Virus Thymidine Kinase-Mediated Suicide Gene Therapy Using Nano/microbubbles and Ultrasound. Ultrasound. *Med. Biol.*,（in press）.
（4）Koshiyama, K., Kodama, T., Yano, T. and Fujikawa, S., Structural Change in Lipid Bilayers and Water Penetration Induced by Shock Waves: Molecular Dynamics Simulations. *Biophys. J.*, **91**-6（2006），2198-2205.